Editors' Suggestion | Featured in Physics

Microwave Quantum Link between Superconducting Circuits Housed in Spatially Separated Cryogenic Systems

P. Magnard,[1,*] S. Storz,[1] P. Kurpiers,[1] J. Schär,[1] F. Marxer,[1] J. Lütolf,[1] T. Walter,[1] J.-C. Besse,[1] M. Gabureac,[1] K. Reuer,[1] A. Akin,[1] B. Royer,[2,‡] A. Blais,[2,3] and A. Wallraff[1,4,†]

[1]*Department of Physics, ETH Zürich, CH-8093 Zürich, Switzerland*

[2]*Institut Quantique and Département de Physique, Université de Sherbrooke, Sherbrooke, Québec J1K 2R1, Canada*

[3]*Canadian Institute for Advanced Research, Toronto, Ontario M5G 1Z8, Canada*

[4]*Quantum Center, ETH Zürich, 8093 Zürich, Switzerland*

(Received 7 August 2020; accepted 16 November 2020; published 21 December 2020)

Superconducting circuits are a strong contender for realizing quantum computing systems and are also successfully used to study quantum optics and hybrid quantum systems. However, their cryogenic operation temperatures and the current lack of coherence-preserving microwave-to-optical conversion solutions have hindered the realization of superconducting quantum networks spanning different cryogenic systems or larger distances. Here, we report the successful operation of a cryogenic waveguide coherently linking transmon qubits located in two dilution refrigerators separated by a physical distance of five meters. We transfer qubit states and generate entanglement on demand with average transfer and target state fidelities of 85.8% and 79.5%, respectively, between the two nodes of this elementary network. Cryogenic microwave links provide an opportunity to scale up systems for quantum computing and create local area superconducting quantum communication networks over length scales of at least tens of meters.

DOI: 10.1103/PhysRevLett.125.260502

Superconducting circuits are an appealing platform to execute quantum information processing algorithms on noisy-intermediate-scale or error-correctable quantum hardware [1–5] and to study fundamental quantum phenomena [6–9]. Today's state-of-the-art superconducting quantum processors contain a few dozen qubits on a single chip, held at cryogenic temperatures in individual dilution refrigerators. Efforts in qubit integration and packaging [10–13] will likely extend the scale of these processors to thousands of qubits in the foreseeable future. However, limitations such as available wafer size, refrigerated space, and cooling power may arise beyond that scale [14]. Therefore, major innovations in both device integration and cryogenics are required to realize error-corrected quantum computers able to tackle interesting problems intractable on high-performance computing systems, likely requiring millions of qubits [15,16]. Networking quantum processors housed in different cryogenic nodes may provide a modular solution to scale up quantum computers beyond these limitations [17,18]. The capabilities of quantum computers may be extended by forming clusters of networked processors housed in individual cryogenic modules similar to the clusters of processing units used in the high-performance systems.

One approach to realize such networks is to use microwave-to-optical quantum transducers [19–22] with which superconducting circuits may be entangled with optical photons to communicate over long distances in a fashion similar to single atoms [23], trapped ions [24], or defects in diamond [25]. However, despite the constant improvement of microwave-to-optical transducers, bringing their conversion efficiency, bandwidth, added noise, laser-induced quasiparticle poisoning, and heat loads to practical levels on a single device remains a challenge.

A complementary approach is to connect dilution-refrigerator-based cryogenic systems with cold, superconducting waveguides [26]. This approach could prove advantageous for distributing quantum computing tasks in local cryogenic quantum networks, as it would benefit from readily available, fast, deterministic, error-correctable, and high-fidelity chip-to-chip quantum communication schemes with microwave photons [26–34]. In this Letter, we report the realization of such a cryogenic quantum microwave channel between superconducting qubits located in two distinct dilution refrigerator units. Using a photon shaping technique to transfer excitations deterministically [28,35], we transfer qubit states and generate entanglement on demand between the distant qubits.

Our experimental setup consists of two cryogen-free dilution refrigerators, each of which houses a superconducting circuit with a single qubit cooled to below 20 mK and separated by 5 m (Fig. 1). The two identically designed circuits have a frequency-tunable transmon qubit, each with relaxation and coherence times $T_1 \simeq 12\ \mu$s and $T_2^e \simeq 6\ \mu$s, coupled dispersively to two Purcell filtered resonators: one for readout and one for excitation transfer, as shown in green and yellow, respectively, in Fig. 1(b). The $|g\rangle$ to $|e\rangle$ transition frequencies of transmon qubits labeled A and B are tuned to $\omega_{q,A}/2\pi = 6.457$ GHz and

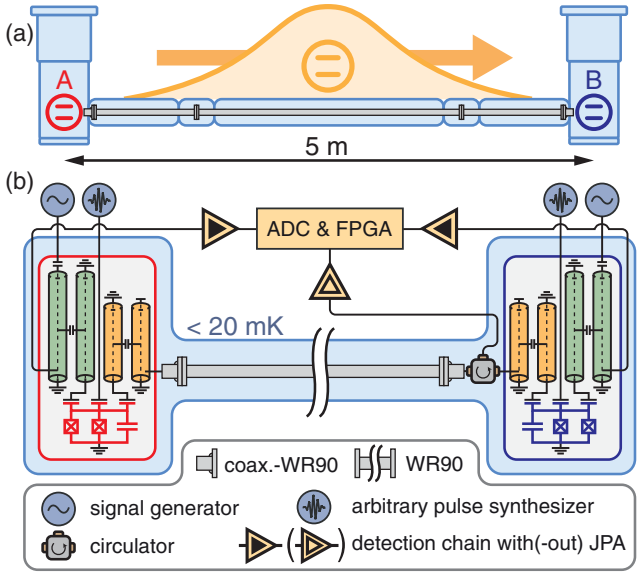

FIG. 1. (a) Schematic representation and (b) simplified circuit diagram of the experimental setup. Each transmon qubit at nodes A (red) and B (blue) is connected to two Purcell filtered $\lambda/4$ resonators: one for readout (green) and one for excitation transfer by emission of a shaped photon (yellow). The light blue background illustrates the refrigerated space.

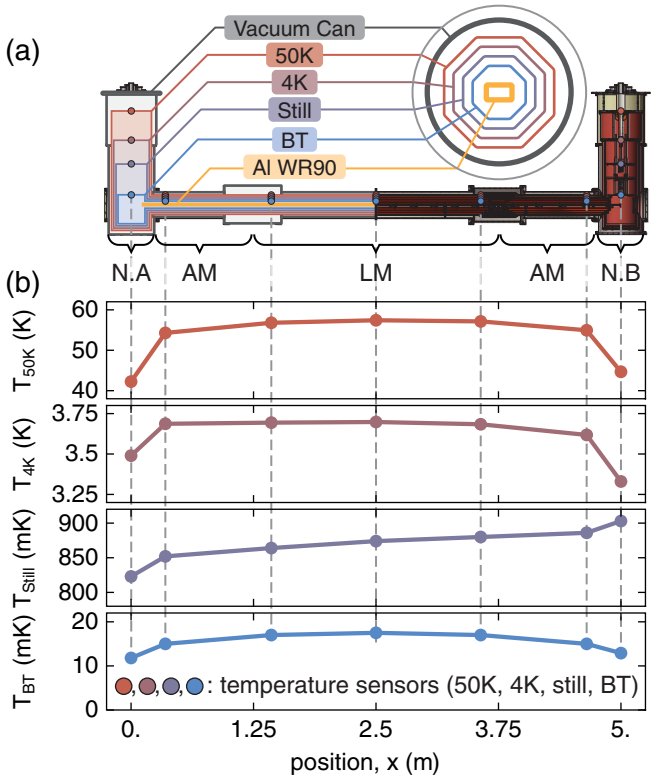

FIG. 2. (a) Longitudinal cross section of a schematic representation (left half) and a 3D model (right half) of the cryogenic system. The inset on the top right shows a transverse cross section of the link. (b) Measured temperature in steady-state vs sensor position x on the axis along the link for all four temperature stages. Nodes A and B: NA and NB; adapter module: AM; link module: LM.

$\omega_{q,B}/2\pi = 6.074$ GHz, respectively, by applying a magnetic field to their superconducting quantum interference device loops. This adjusts the dispersive shift on each transfer resonator such that their frequencies $\omega_t/2\pi = 8.406$ GHz are matched [28]. Here, $|g\rangle$, $|e\rangle$, and $|f\rangle$ denote the three lowest energy levels of the transmon qubit.

We connect the transfer resonators to each other through a 4.9 m long, superconducting, rectangular aluminum WR90 waveguide in series with two flexible, coaxial copper cables of 0.4 m length each and a circulator. At mK temperatures, the waveguide exhibits attenuation below 1 dB/km over the X band (8–12 GHz), which amounts to a total loss below 10^{-3} over 4.9 m of the waveguide [36]. With attenuation levels comparable to that of optical photons in telecom fibers [44], the waveguide is in principle suited for high-fidelity transmission of microwave photons over intracity scale distances [26].

To perform single-qubit gates, we apply microwave pulses created by arbitrary waveform generators to each qubit through dedicated drive lines. To perform readout, we apply a gated microwave tone to the readout resonator. The transmitted signal is then amplified, down-converted, digitized, and processed by a field-programmable gate array (FPGA). Using quantum-limited Josephson parametric amplifiers (JPA) in the detection chain, we achieve single-shot three-level discrimination of the transmon states with ~5% average error (10% for joint two-qubit readout). Devices, microwave setup, pulse calibration, and qubit readout are discussed in more detail in the Supplemental Material [36].

We cool the waveguide to temperatures below 20 mK by mounting it in a custom-made cryogenic system consisting of concentric, octagonal radiation shields held at temperatures of approximately 50 K, 4 K, 850 mK (still), and 15 mK (base temperature) and installed in an o-ring sealed vacuum can [Fig. 2(a)]. See the Supplemental Material for a photograph of the full system [36]. The waveguide is thermalized to the base temperature shield every 0.25 m using flexible copper braids, and the radiation shields are cooled to their equilibrium temperatures using the dilution refrigerators at each end of the system.

The largest heat load on the system is due to room temperature black body radiation, which we mitigate by a set of low-emissivity radiation shields manufactured from high thermal conductivity copper and mechanically supported by thin-walled low thermal conductivity posts. In addition, the heat load on the 50 K stage is reduced by using multilayer insulation [45]. Generally, minimizing the heat flow between shields at different temperature stages and maximizing the thermal conductivity along each stage reduces thermal gradients and thus allows for lower final temperatures. By making the arrangement of shields lightproof, the base temperature shields cool to below 20 mK.

We designed the link to be modular, with 1.25 m long adapter modules to connect the link to each dilution refrigerator and 2.5 m long link modules, which also allow for an extension of the link [Fig. 2(a)]. To compensate for thermal contraction during cooldown, we use flexible copper braids for thermal anchoring between modules. For the same reason, flexible coaxial cables are used to connect the samples to the waveguide.

To monitor the temperature profile of the link, we installed temperature sensors at the positions indicated in Fig. 2(a). Three days after commencing cooldown, the system reaches the steady-state temperature distribution shown in Fig. 2(b), demonstrating the excellent performance of the system. As expected, on each stage, the temperature is lowest at the nodes and the highest in the middle of the link, with an exception for the still stage where we heated node B to 900 mK to optimize cooling power by increasing the flow of ^{3}He.

To characterize the excitation transfer through the link, we first reset the transmon qubits with microwave drives [46] and apply two consecutive Gaussian π pulses to prepare the qubit and resonator system at node A in the state $|f0\rangle$ [Fig. 3(a)], where $|q\rangle$ and $|n\rangle$ in $|qn\rangle$ denote the transmon state and the transfer resonator Fock state, respectively. We then drive transmon A on the $|f0\rangle \leftrightarrow |g1\rangle$ sideband transition [47,48] to populate the transfer resonator with one photon. This photon couples into the waveguide at rate $\kappa_A/2\pi = 8.9$ MHz and propagates to node B in 28 ns, as estimated from the waveguide length and the relevant group velocities [36]. We shape the $|f0\rangle \leftrightarrow |g1\rangle$ pulse appropriately to emit the photon with a time-symmetric envelope $\phi(t) \propto \mathrm{sech}(\Gamma t/2)$ [28,48,49], where the photon bandwidth Γ can be adjusted up to a maximum value of $\min[\kappa_A, \kappa_B]$. Here we choose $\Gamma/2\pi = \kappa_B/2\pi \simeq 6.2$ MHz to minimize the duration of the protocol. To absorb the photon at node B, we then drive transmon B with an $|f0\rangle \leftrightarrow |g1\rangle$ pulse whose time reverse would emit a photon indistinguishable from the incoming one [35]. Finally, we apply an e-f π pulse on transmon B to map the excitation back to the g-e manifold and then perform a single-shot readout on both qutrits. Here and in following experiments, we present data that is corrected for readout errors using reference measurements [36]. For these parameters, the excitation transfer sequence, consisting of the $|f0\rangle \leftrightarrow |g1\rangle$ pulses and the final e-f π pulse, completes in 311 ns.

Truncating the $|f0\rangle \leftrightarrow |g1\rangle$ pulses prematurely at time τ, we characterize the time dependence of the state population of the two transmon qubits throughout the transfer pulse (Fig. 3). As the excitation transfers from node A to node B via the photonic modes (the waveguide and both transfer resonators), the population swaps from the state $|fg\rangle$ of the two spatially separated qubits $|AB\rangle$ to $|ge\rangle$ via the intermediate state $|gg\rangle$. The final two-transmon state populations highlight the different sources of errors in the excitation transfer. The ~3% residual

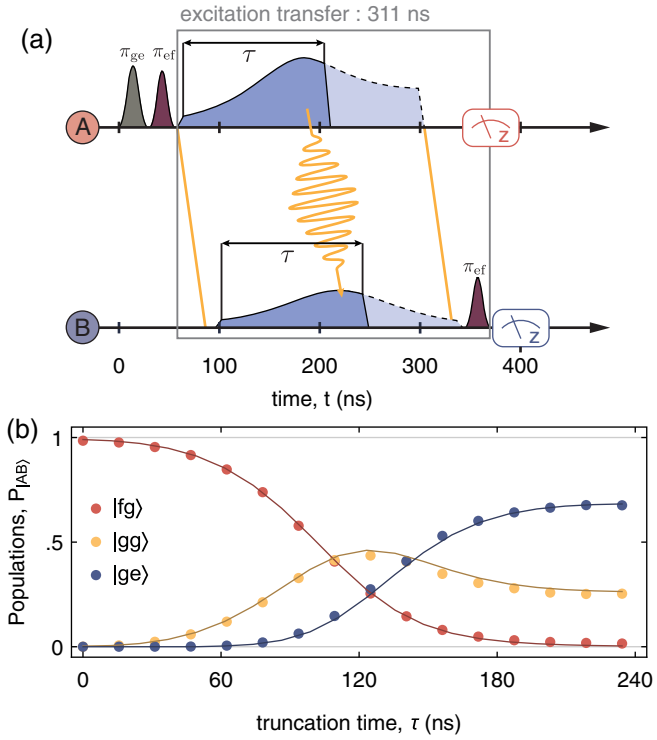

FIG. 3. (a) Pulse scheme used to characterize the excitation transfer dynamics. The $|f0\rangle \rightarrow |g1\rangle$ drives and the g-e and e-f π pulses are represented in blue, gray, and purple, respectively. We use solid and dashed lines for the time-truncated ($\tau = 140$ ns) and full excitation transfer sequences, respectively. The straight yellow lines illustrate the propagation path of the rising and falling edges of the photon in space-time. The subsequence defining the excitation transfer is enclosed in a gray box. (b) Population P in selected two-transmon states $|AB\rangle$ vs $|f0\rangle \leftrightarrow |g1\rangle$ pulse truncation time τ. Solid lines show the results of master equation simulations.

population measured in both $|gf\rangle$ and $|eg\rangle$ (not shown) is due to e-f decay. In case of photon loss or failed absorption during the transfer process, the system ends up in the state $|gg\rangle$. Comparing the measured amplitudes of the fields emitted by A or B using the measurement chain behind the circulator [Fig. 1(b)], we determine a 22.3% photon loss, dominated by the insertion loss of the circulator, and a 4.2% absorption inefficiency [36], which is in reasonable agreement with the 25.3% residual population measured in the state $|gg\rangle$. Finally, the transfer efficiency is characterized by the 67.5% final population in $|ge\rangle$. The time between the applications of the emission and absorption pulses is set to experimentally maximize the transfer efficiency. By comparing the time of arrival of photons emitted from A or B in the photon measurement chain, we determine this optimal time difference to be 38 ns, which decomposes into the photon propagation time and an extra 10 ns lag [36]. Simulations of the transfer dynamics, using the master equation model from Ref. [28] and independently measured parameters, are in

good agreement with the data [solid lines in Fig. 3(b)] and the measured pulse timing [36].

To probe the quantum nature of the excitation transfer, we characterize the qubit state transfer protocol with quantum process tomography. To do so, we reset the qubits to their ground states, prepare A in one of the six mutually unbiased qubit states [50], apply an e-f π pulse on A, and then apply an excitation transfer sequence [Fig. 4(a)]. For each input state $\rho_{i,s}$ we reconstruct the final state $\rho_{f,s}$ of transmon B with three-level quantum state tomography, from which we infer the transfer process matrix χ [36]. We determine an average state fidelity $\mathcal{F}_s = \frac{1}{6}\sum_s \mathcal{F}(\rho_{i,s},\rho_{f,s}) = 82.4 \pm 0.06\%$ and a process fidelity of $\mathcal{F}_p = \mathrm{Tr}(\chi_{\mathrm{ideal}}\chi) = 75.3 \pm 0.1\%$ relative to the ideal qubit state transfer process. When correcting for readout errors, these fidelities reach $85.8 \pm 0.06\%$ and $79.5 \pm 0.1\%$, respectively [Fig. 4(b)]. On average, the input states have equal populations in $|g\rangle$ and $|e\rangle$, which are transferred in vacuum states, insensitive to loss, with close-to-unit fidelity, and single-photon Fock states, suffering from loss, with a fidelity of 67.5% corresponding to the transfer efficiency. Therefore, the state transfer fidelities $\mathcal{F}_s$ and $\mathcal{F}_p$ can be larger than the photon transfer efficiency if the phase coherence of the process is sufficiently large.

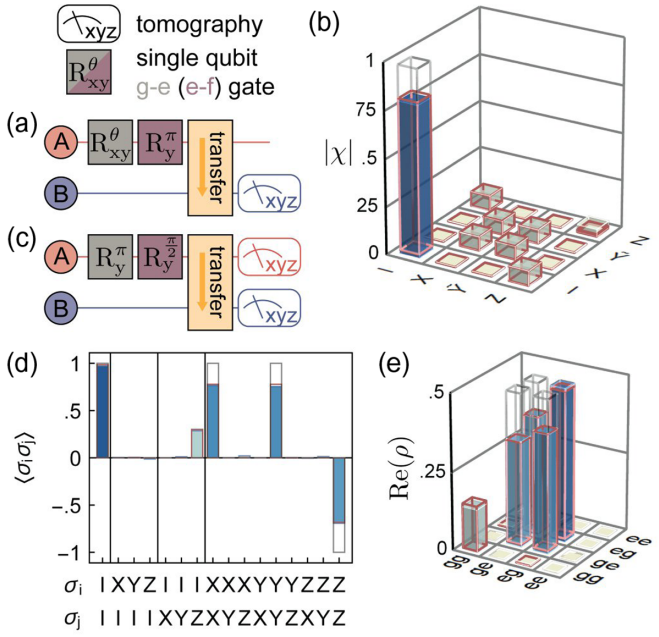

FIG. 4. (a) Quantum circuit used to perform and characterize the qubit state transfer. (b) Absolute value of the qubit state transfer matrix $|\chi|$ in the Pauli basis $\{\mathbb{1}, X = \hat{\sigma}_x, \tilde{Y} = i\hat{\sigma}_y, Z = \hat{\sigma}_z\}$. (c) Quantum circuit used to deterministically generate and characterize the Bell state $|\psi^+\rangle$. (d) Expectation value $\langle\sigma_i\sigma_j\rangle$ of the two-qubit Pauli operators, and (e) real part of the density matrix ρ of reconstructed Bell state. In (b),(d),(e), solid blue bars, red wireframes, and gray wireframes are the measured, simulated, and target quantities, respectively.

To generate entanglement across the link, we prepare qubit A in $(|e\rangle + |f\rangle)/\sqrt{2}$, qubit B in $|g\rangle$, and apply the excitation transfer pulses [Fig. 4(c)]. Using quantum state tomography, we reconstruct the two-qutrit density matrix $\rho_{3\otimes 3}$ of qubits A and B [36]. To quantify the entanglement with standard metrics, we consider the density matrix ρ, consisting of the two-qubit elements of $\rho_{3\otimes 3}$ [Fig. 4(d),(e)]. We determine the fidelity $\langle\psi^+|\rho|\psi^+\rangle = 79.5 \pm 0.1\%$ $(71.9 \pm 0.1\%)$ with respect to the ideal Bell state $|\psi^+\rangle = (|ge\rangle + |eg\rangle)/\sqrt{2}$, and evaluate a concurrence of $\mathcal{C}(\rho) = 0.746 \pm 0.003$ (0.588 ± 0.002), with (without) correction for readout errors.

Simulations of the qubit state transfer and entanglement generation sequences are in good agreement with the measurement results, as quantified by the small trace distances $\sqrt{\mathrm{Tr}(|\chi - \chi_{\mathrm{sim}}|^2)} = 0.09$ and $\sqrt{\mathrm{Tr}(|\rho - \rho_{\mathrm{sim}}|^2)} = 0.023$ between the reconstructed and simulated quantities. These simulations suggest that photon loss and transmon decay are the dominant sources of errors in these protocols, contributing to 11.8% and ~6% infidelity, respectively. In future experiments, the photon loss may be reduced to 5% by removing the circulator [31–34], by using a printed circuit board metalized with a superconductor, and by using low-loss coaxial cables between the device and the waveguide. Simulations of the protocols with 5% photon loss and reasonably improved coherence times $(T_1 \simeq T_2^e \simeq 30\ \mu\mathrm{s})$ and transfer resonator bandwidth $(\kappa/2\pi = 12\ \mathrm{MHz})$ indicate that Bell state fidelities and state transfer process fidelities as high as 96% may be achievable, which may enable distributed surface-code computation [17] and communication [51] between distant cryogenic nodes. Further improvement may be obtainable using protocols requiring less time compared to the coherence of the circuit elements [31] or ones that are resilient to photon loss [33,34,52,53] and thermal excitation [26,27].

This realization of a meter-scale, mK temperature, microwave-frequency coherent quantum link and its use for quantum state transfer and entanglement generation suggests a number of directions for future research. For example, we plan to experimentally investigate the distribution of quantum information processing tasks between quantum nodes hosting multiple qubits using a coherent cryogenic network, an essential part of a modular quantum computer architecture [54]. In addition, the modularity of the cryogenic link demonstrated here offers a straightforward path toward extending the physical distance between nodes by adding modules to the link. Due to the small photon loss in the superconducting rectangular waveguide, cryogenic links covering distances of tens or even hundreds of meters could be realized, primarily limited by financial constraints imposed by the thermal requirements. On such length scales, one may investigate nonlocal physics [55,56] or non-Markovian waveguide QED [57,58] with superconducting quantum devices and set the grounds for microwave quantum local area networks [26].

This work is supported by the European Research Council (ERC) through the "Superconducting Quantum Networks" (SuperQuNet) project, by the National Centre of Competence in Research "Quantum Science and Technology" (NCCR QSIT), a research instrument of the Swiss National Science Foundation (SNSF), by ETH Zurich, by NSERC, the Canada First Research Excellence Fund, and by the Vanier Canada Graduate Scholarships. P. M., S. S., P. K. and T. W. designed and developed the experiment. J.-C. B., T. W. and M. G. fabricated the samples. J. L., P. K., P. M., S. S., F. M., and J. S. designed, characterized, and assembled the cryogenic system. P. M., P. K., and S. S. performed the experiments. P. M., P. K., and A. W. analyzed and interpreted the data. P. M., K. R, A. A., J. S., and F. M. implemented the FPGA firmware and experiment automation. B. R., P. M., and P. K. performed the master equation simulations. P. M. and A. W. wrote the manuscript. All authors commented on the manuscript. The project was led by A. W.

*Corresponding author.
paul.magnard@phys.ethz.ch
†Corresponding author.
andreas.wallraff@phys.ethz.ch
‡Present Address: Department of Physics, Yale University, New Haven, Connecticut 06520, USA.

[1] J. Preskill, Quantum computing in the NISQ era and beyond, Quantum **2**, 79 (2018).
[2] F. Arute *et al.*, Quantum supremacy using a programmable superconducting processor, Nature (London) **574**, 505 (2019).
[3] A. Kandala, K. Temme, A. D. Córcoles, A. Mezzacapo, J. M. Chow, and J. M. Gambetta, Error mitigation extends the computational reach of a noisy quantum processor, Nature (London) **567**, 491 (2019).
[4] N. Ofek, A. Petrenko, R. Heeres, P. Reinhold, Z. Leghtas, B. Vlastakis, Y. Liu, L. Frunzio, S. M. Girvin, L. Jiang, M. Mirrahimi, M. H. Devoret, and R. J. Schoelkopf, Extending the lifetime of a quantum bit with error correction in superconducting circuits, Nature (London) **536**, 441 (2016).
[5] C. K. Andersen, A. Remm, S. Lazar, S. Krinner, N. Lacroix, G. J. Norris, M. Gabureac, C. Eichler, and A. Wallraff, Repeated quantum error detection in a surface code, Nat. Phys. **16**, 875 (2020).
[6] A. van Loo, A. Fedorov, K. Lalumière, B. Sanders, A. Blais, and A. Wallraff, Photon-mediated interactions between distant articial atoms, Science **342**, 1494 (2013).
[7] S. Hacohen-Gourgy, L. S. Martin, E. Flurin, V. V. Ramasesh, K. B. Whaley, and I. Siddiqi, Quantum dynamics of simultaneously measured non-commuting observables, Nature (London) **538**, 491 (2016).
[8] N. Cottet, S. Jezouin, L. Bretheau, P. Campagne-Ibarcq, Q. Ficheux, J. Anders, A. Auffèves, R. Azouit, P. Rouchon, and B. Huard, Observing a quantum maxwell demon at work, Proc. Natl. Acad. Sci. U.S.A. **114**, 7561 (2017).
[9] Z. K. Minev, S. O. Mundhada, S. Shankar, P. Reinhold, R. Gutiérrez-Jáuregui, R. J. Schoelkopf, M. Mirrahimi, H. J. Carmichael, and M. H. Devoret, To catch and reverse a quantum jump mid-flight, Nature (London) **570**, 200 (2019).
[10] J. H. Béjanin, T. G. McConkey, J. R. Rinehart, C. T. Earnest, C. R. H. McRae, D. Shiri, J. D. Bateman, Y. Rohanizadegan, B. Penava, P. Breul, S. Royak, M. Zapatka, A. G. Fowler, and M. Mariantoni, Three-Dimensional Wiring for Extensible Quantum Computing: The Quantum Socket, Phys. Rev. Applied **6**, 044010 (2016).
[11] R. N. Das, J. L. Yoder, D. Rosenberg, D. K. Kim, D. Yost, J. Mallek, D. Hover, V. Bolkhovsky, A. J. Kerman, and W. D. Oliver, Cryogenic qubit integration for quantum computing, in *IEEE 68th Electronic Components and Technology Conference (ECTC)* (IEEE, San Diego, CA, 2018), https://dx.doi.org./10.1109/ECTC.2018.00080.
[12] B. Foxen *et al.*, Qubit compatible superconducting interconnects, Quantum Sci. Technol. **3**, 014005 (2018).
[13] C. U. Lei, L. Krayzman, S. Ganjam, L. Frunzio, and R. J. Schoelkopf, High coherence superconducting microwave cavities with indium bump bonding, Appl. Phys. Lett. **116**, 154002 (2020).
[14] S. Krinner, S. Storz, P. Kurpiers, P. Magnard, J. Heinsoo, R. Keller, J. Lütolf, C. Eichler, and A. Wallraff, Engineering cryogenic setups for 100-qubit scale superconducting circuit systems, Eur. Phys. J. Quantum Technol. **6**, 2 (2019).
[15] M. Reiher, N. Wiebe, K. M. Svore, D. Wecker, and M. Troyer, Elucidating reaction mechanisms on quantum computers, Proc. Natl. Acad. Sci. U.S.A. **114**, 7555 (2017).
[16] R. Babbush, C. Gidney, D. W. Berry, N. Wiebe, J. McClean, A. Paler, A. Fowler, and H. Neven, Encoding Electronic Spectra in Quantum Circuits with Linear T Complexity, Phys. Rev. X **8**, 041015 (2018).
[17] N. H. Nickerson, J. F. Fitzsimons, and S. C. Benjamin, Freely Scalable Quantum Technologies Using Cells of 5-to-50 Qubits with Very Lossy and Noisy Photonic Links, Phys. Rev. X **4**, 041041 (2014).
[18] T. Brecht, W. Pfaff, C. Wang, Y. Chu, L. Frunzio, M. H. Devoret, and R. J. Schoelkopf, Multilayer microwave integrated quantum circuits for scalable quantum computing, npj Quantum Inf. **2**, 16002 (2016).
[19] L. Fan, C.-L. Zou, R. Cheng, X. Guo, X. Han, Z. Gong, S. Wang, and H. X. Tang, Superconducting cavity electro-optics: A platform for coherent photon conversion between superconducting and photonic circuits, Sci. Adv. **4**, eaar4994 (2018).
[20] A. P. Higginbotham, P. S. Burns, M. D. Urmey, R. W. Peterson, N. S. Kampel, B. M. Brubaker, G. Smith, K. W. Lehnert, and C. A. Regal, Harnessing electro-optic correlations in an efficient mechanical converter, Nat. Phys. **14**, 1038 (2018).
[21] M. Forsch, R. Stockill, A. Wallucks, I. Marinković, C. Gärtner, R. A. Norte, F. van Otten, A. Fiore, K. Srinivasan, and S. Gröblacher, Microwave-to-optics conversion using a mechanical oscillator in its quantum ground state, Nat. Phys. **16**, 69 (2020).
[22] M. Mirhosseini, A. Sipahigil, M. Kalaee, and O. Painter, Quantum transduction of optical photons from a superconducting qubit, arXiv:2004.04838.
[23] J. Hofmann, M. Krug, N. Ortegel, L. Gérard, M. Weber, W. Rosenfeld, and H. Weinfurter, Heralded entanglement

between widely separated atoms, Science **337**, 72 (2012).

[24] D. L. Moehring, P. Maunz, S. Olmschenk, K. C. Younge, D. N. Matsukevich, L. M. Duan, and C. Monroe, Entanglement of single-atom quantum bits at a distance, Nature (London) **449**, 68 (2007).

[25] H. Bernien, B. Hensen, W. Pfaff, G. Koolstra, M. S. Blok, L. Robledo, T. H. Taminiau, M. Markham, D. J. Twitchen, L. Childress, and R. Hanson, Heralded entanglement between solid-state qubits separated by three metres, Nature (London) **497**, 86 (2013).

[26] Z.-L. Xiang, M. Zhang, L. Jiang, and P. Rabl, Intracity Quantum Communication via Thermal Microwave Networks, Phys. Rev. X **7**, 011035 (2017).

[27] B. Vermersch, P.-O. Guimond, H. Pichler, and P. Zoller, Quantum State Transfer via Noisy Photonic and Phononic Waveguides, Phys. Rev. Lett. **118**, 133601 (2017).

[28] P. Kurpiers, P. Magnard, T. Walter, B. Royer, M. Pechal, J. Heinsoo, Y. Salathé, A. Akin, S. Storz, J.-C. Besse, S. Gasparinetti, A. Blais, and A. Wallraff, Deterministic quantum state transfer and remote entanglement using microwave photons, Nature (London) **558**, 264 (2018).

[29] P. Campagne-Ibarcq, E. Zalys-Geller, A. Narla, S. Shankar, P. Reinhold, L. Burkhart, C. Axline, W. Pfaff, L. Frunzio, R. J. Schoelkopf, and M. H. Devoret, Deterministic Remote Entanglement of Superconducting Circuits Through Microwave Two-Photon Transitions, Phys. Rev. Lett. **120**, 200501 (2018).

[30] C. Axline, L. Burkhart, W. Pfaff, M. Zhang, K. Chou, P. Campagne-Ibarcq, P. Reinhold, L. Frunzio, S. M. Girvin, L. Jiang, M. H. Devoret, and R. J. Schoelkopf, On-demand quantum state transfer and entanglement between remote microwave cavity memories, Nat. Phys. **14**, 705 (2018).

[31] Y. P. Zhong, H.-S. Chang, K. J. Satzinger, M.-H. Chou, A. Bienfait, C. R. Conner, É. Dumur, J. Grebel, G. A. Peairs, R. G. Povey, D. I. Schuster, and A. N. Cleland, Violating Bell's inequality with remotely connected superconducting qubits, Nat. Phys. **15**, 741 (2019).

[32] N. Leung, Y. Lu, S. Chakram, R. K. Naik, N. Earnest, R. Ma, K. Jacobs, A. N. Cleland, and D. I. Schuster, Deterministic bidirectional communication and remote entanglement generation between superconducting qubits, npj Quantum Inf. **5**, 18 (2019).

[33] H.-S. Chang, Y. P. Zhong, A. Bienfait, M.-H. Chou, C. R. Conner, E. Dumur, J. Grebel, G. A. Peairs, R. G. Povey, K. J. Satzinger, and A. N. Cleland, Remote Entanglement via Adiabatic Passage Using a Tunably Dissipative Quantum Communication System, Phys. Rev. Lett. **124**, 240502 (2020).

[34] L. D. Burkhart, J. Teoh, Y. Zhang, C. J. Axline, L. Frunzio, M. H. Devoret, L. Jiang, S. M. Girvin, and R. J. Schoelkopf, Error-detected state transfer and entanglement in a superconducting quantum network, arXiv:2004.06168.

[35] J. I. Cirac, P. Zoller, H. J. Kimble, and H. Mabuchi, Quantum State Transfer and Entanglement Distribution Among Distant Nodes in a Quantum Network, Phys. Rev. Lett. **78**, 3221 (1997).

[36] See Supplemental Material, which includes Refs. [37–43], at http://link.aps.org/supplemental/10.1103/PhysRevLett.125.260502 for details about the characterization of waveguide loss, for details about the sample fabrication and parameters, for a complete wiring diagram of the setup, for details about the calibration of pulses and their relative timings, for details about qutrit single-shot readout, for a photograph of the full cryogenic system, for details about the characterization of some properties of the transfer via measurement of photon envelopes, and for details about the tomographic reconstruction methods.

[37] P. Kurpiers, T. Walter, P. Magnard, Y. Salathe, and A. Wallraff, Characterizing the attenuation of coaxial and rectangular microwave-frequency waveguides at cryogenic temperatures, Eur. Phys. J. Quantum Technol. **4**, 8 (2017).

[38] D. M. Pozar, *Microwave Engineering*, 4th ed. (Wiley & Sons, Inc., New Jersey, USA, 2012).

[39] T. Walter, P. Kurpiers, S. Gasparinetti, P. Magnard, A. Potočnik, Y. Salathé, M. Pechal, M. Mondal, M. Oppliger, C. Eichler, and A. Wallraff, Rapid, High-Delity, Single-Shot Dispersive Readout of Superconducting Qubits, Phys. Rev. Applied **7**, 054020 (2017).

[40] K. Geerlings, Z. Leghtas, I. M. Pop, S. Shankar, L. Frunzio, R. J. Schoelkopf, M. Mirrahimi, and M. H. Devoret, Demonstrating a Driven Reset Protocol for a Superconducting Qubit, Phys. Rev. Lett. **110**, 120501 (2013).

[41] K. Serniak, M. Hays, G. de Lange, S. Diamond, S. Shankar, L. D. Burkhart, L. Frunzio, M. Houzet, and M. H. Devoret, Hot Nonequilibrium Quasiparticles in Transmon Qubits, Phys. Rev. Lett. **121**, 157701 (2018).

[42] F. Motzoi, J. M. Gambetta, P. Rebentrost, and F. K. Wilhelm, Simple Pulses for Elimination of Leakage in Weakly Nonlinear Qubits, Phys. Rev. Lett. **103**, 110501 (2009).

[43] I. L. Chuang and M. A. Nielsen, Prescription for experimental determination of the dynamics of a quantum black box, J. Mod. Opt. **44**, 2455 (1997).

[44] Y. Tamura, H. Sakuma, K. Morita, M. Suzuki, Y. Yamamoto, K. Shimada, Y. Honma, K. Sohma, T. Fujii, and T. Hasegawa, The first 0.14-db/km loss optical fiber and its impact on submarine transmission, J. Light. Technol. **36**, 44 (2018).

[45] V. Parma, Cryostat Design, CAS—CERN Accelerator School: Course on Superconductivity for Accelerators, https://doi.org/10.5170/CERN-2014-005.353 (2014).

[46] P. Magnard, P. Kurpiers, B. Royer, T. Walter, J.-C. Besse, S. Gasparinetti, M. Pechal, J. Heinsoo, S. Storz, A. Blais, and A. Wallraff, Fast and Unconditional All-Microwave Reset of a Superconducting Qubit, Phys. Rev. Lett. **121**, 060502 (2018).

[47] S. Zeytinoğlu, M. Pechal, S. Berger, A. A. Abdumalikov Jr., A. Wallraff, and S. Filipp, Microwave-induced amplitude- and phase-tunable qubit-resonator coupling in circuit quantum electrodynamics, Phys. Rev. A **91**, 043846 (2015).

[48] M. Pechal, L. Huthmacher, C. Eichler, S. Zeytinoğlu, A. A. Abdumalikov Jr., S. Berger, A. Wallraff, and S. Filipp, Microwave-Controlled Generation of Shaped Single Photons in Circuit Quantum Electrodynamics, Phys. Rev. X **4**, 041010 (2014).

[49] O. Morin, M. Körber, S. Langenfeld, and G. Rempe, Deterministic Shaping and Reshaping of Single-Photon Temporal Wave Functions, Phys. Rev. Lett. **123**, 133602 (2019).

[50] S. J. van Enk, N. Lütkenhaus, and H. J. Kimble, Experimental procedures for entanglement verication, Phys. Rev. A **75**, 052318 (2007).

[51] A. G. Fowler, D. S. Wang, C. D. Hill, T. D. Ladd, R. Van Meter, and L. C. L. Hollenberg, Surface Code Quantum Communication, Phys. Rev. Lett. **104**, 180503 (2010).

[52] P. Kurpiers, M. Pechal, B. Royer, P. Magnard, T. Walter, J. Heinsoo, Y. Salathé, A. Akin, S. Storz, J.-C. Besse, S. Gasparinetti, A. Blais, and A. Wallraff, Quantum Communication with Time-Bin Encoded Microwave Photons, Phys. Rev. Applied **12**, 044067 (2019).

[53] K. Bergmann *et al.*, Roadmap on STIRAP applications, J. Phys. B **52**, 202001 (2019).

[54] J. I. Cirac, A. K. Ekert, S. F. Huelga, and C. Macchiavello, Distributed quantum computation over noisy channels, Phys. Rev. A **59**, 4249 (1999).

[55] B. Hensen, H. Bernien, A. E. Dreau, A. Reiserer, N. Kalb, M. S. Blok, J. Ruitenberg, R. F. L. Vermeulen, R. N. Schouten, C. Abellan, W. Amaya, V. Pruneri, M. W. Mitchell, M. Markham, D. J. Twitchen, D. Elkouss, S. Wehner, T. H. Taminiau, and R. Hanson, Loophole-free Bell inequality violation using electron spins separated by 1.3 kilometres, Nature (London) **526**, 682 (2015).

[56] P. Bierhorst, E. Knill, S. Glancy, Y. Zhang, A. Mink, S. Jordan, A. Rommal, Y.-K. Liu, B. Christensen, S. W. Nam, M. J. Stevens, and L. K. Shalm, Experimentally generated randomness certified by the impossibility of superluminal signals, Nature (London) **556**, 223 (2018).

[57] F. Dinc and A. M. Branczyk, Non-markovian super-superradiance in a linear chain of up to 100 qubits, Phys. Rev. Research **1**, 032042 (2019).

[58] G. Calajó, Y.-L. L. Fang, H. U. Baranger, and F. Ciccarello, Exciting a bound state in the continuum through multiphoton scattering plus delayed quantum feedback, Phys. Rev. Lett. **122**, 073601 (2019).